Desalination and Water Treatment
www.deswater.com

doi: 10.5004/dwt.2022.28247

250 (2022) 252–265
February

Artificial neural network mathematical modeling of methyl violet removal with chitosan-coated clinoptilolite

Esra Altıntığ[a,*], Onur Kabadayı[b], Dilay Bozdag[c], Selma Altundag[d], Huseyin Altundag[b]

[a]*Chemical and Chemical Processing Technologies Department, Pamukova Vocational School, Sakarya University of Applied Sciences, 54900 Sakarya, Turkey, Tel. +90 5322751726; email: altintig@subu.edu.tr (E. Altıntığ)*
[b]*Department of Chemistry, Faculty of Arts and Sciences, Sakarya University, 54187 Sakarya, Turkey, emails: altundag@sakarya.edu.tr (H. Altundag), kbdyonr@gmail.com (O. Kabadayı)*
[c]*Akcoat Advanced Chemical Coating Materials Industry and Trade Joint Stock Company, 54300 Sakarya, Turkey, email: dilay.bozdag@akcoat.com (D. Bozdag)*
[d]*Department of Mathematics, Faculty of Arts and Sciences, Sakarya University, 54187 Sakarya, Turkey, email: scaylan@sakarya.edu.tr (S. Altundag)*
Received 30 September 2021; Accepted 22 January 2022

ABSTRACT

In this study, the use of chitosan-coated clinoptilolite zeolite as an adsorbents in the removal methyl violet from an aqueous solutions were investigated. Firstly, the structural and chemical characterization of the adsorbent was carried out using various analytical techniques such as X-ray diffraction, Brunauer–Emmett–Teller and scanning electron microscopy. Then, the effects of different batch parameters such as initial pH (2–9), adsorbent dosage (0.05–1.0 g/100 mL), temperature (298–318 K), initial dyestuff concentration (25–125 mg L^{-1}) and mixing time (5–120 min) on the adsorption process were examined. The kinetic, thermodynamic and isotherm parameters of chitosan-coated clinoptilolite zeolite was investigated by batch adsorption experiments. The experimental data showed that the adsorption isotherms were well defined by the Langmuir equilibrium isotherm model equation. The maximum adsorption capacity was found 111.11 mg g^{-1} for chitosan-coated clinoptilolite zeolite adsorbent at 318 K. The methyl violet adsorption was determined to conform to the pseudo-second-order kinetic model. The thermodynamic calculations were made in the adsorption study of chitosan-coated clinoptilolite. As a result of calculations, it was determined that the $\Delta H°$ values were 34.53 kJ mol^{-1}, and the fact that this value is positive indicates that the adsorption process is spontaneous and endothermic. The recovery test exhibited that the developed composite had significantly adsorption/desorption performance particularly until the seventh cycle. In the last step, considering the effects of some experimental parameters on methyl violet adsorption, an artificial neural network model was developed, and it was concluded that it could be used for dye removal from aqueous solutions. All experimental studies showed that found to be a natural, cost-efficient and eco-friendly of the developed chitosan coating on clinoptilolite zeolite composite make it economic easily applicable adsorbent in the removal of methyl violet from the aqueous solutions.

Keywords: Methyl violet; Adsorption; Chitosan; Clinoptilolite; Artificial neural network modeling

1. Introduction

* Corresponding author.

Dyestuffs are commonly used as coloring agents in the textile, printing, rubber, cosmetics, plastic, and leather industries [1,2]. Since dyestuffs are dissolved in water and generate very bright colors due to their acidic character, depolarization of the discharge waters from the textile and production industries is a primary problem for environmental managers, and also pose significant problems for countries [3–5]. In addition, the pH value of water replacements and chemical oxygen demand of water (COD) due to their increase, even at very low concentrations, the human an important environmental problem for health and aquatic life they are the cause [2,6]. The methyl violet, one of these dyestuffs, is generally used in textiles, printing, classification of bacteria and disinfectant [3,5]. The ingestion of methyl violet irritates the gastrointestinal tract, while inhalation irritates the respiratory tract. The methyl violet is difficult to degrade due to three phenyl groups, each bonded to a nitrogen atom that interacts with one or two methyl groups [5]. In the literature, different techniques have been used to remove dyes from aqueous solutions. One of the most common methods used to remove these pollutants from wastewater is the adsorption method, which is a well-known equilibrium separation process and is effective in removing pollutants from waste [6]. With adsorption processes carried out using a natural adsorbent for the removal of dyestuffs related studies are gradually increasing [5,7]. Among the natural materials used, bentonite [8], kaolin [9], activated carbon [10], it contains vermiculite [11], zeolites [12,13], chitin and chitosan [14–19]. The chitosan is a deacetylated product of N-acetyl-D-glucopyranose, the chemical structure of which is similar to cellulose, the most common after cellulose in nature. The chemical structures of chitin and chitosan are shown in Fig. S1. Chitosan is used in the adsorption process due to the functional amino and hydroxyl groups present on its surface [14]. However, only pure chitosan has a low specific gravity the height of the price, it has disadvantages, such as having poor chemical and mechanical properties [20–23]. This therefore, in practical applications, chitosan is modified with natural adsorbents such as zeolite to increase its chemical and physical resistance [22–24]. Zeolites are high porosity materials with different pore structures formed by a three-dimensional SiO_4 and AlO_4 tetrahedron. The SiO_4 tetrahedral part is negative and when it is replaced with Si^{4+} in the center of the Al^{3+} tetrahedral structure, it loads the weak cationic structure stored in the pores negatively and the negative load is balanced by cations [9–13]. The clinoptilolite, which is a kind of natural zeolite that we also used in our study, is widely available in the world and in Turkey. It is also one of the most preferred among all other types of natural zeolite due to its high ion exchange and adsorption properties [25,26]. In addition, the low cost and availability of clinoptilolites make it attractive for use in a variety of environmental applications. Clinoptilolite is used in the adsorption of various dyestuffs such as reactive, anionic, cationic, and phenothiazine from aquatic environments [11–13].

The experimental approach is important from both a time and an economic point of view. Therefore, in order to avoid the troubles that arise during the experiment, the modeling approach is a good solution. Artificial neural networks (ANN), one of the features of based modeling, does not require mathematical knowledge [27]. Therefore, the description of events in the process of it is a useful method for simulation and scaling of complex adsorption systems. ANN are now commonly used in many areas of chemistry [27,28]. ANN, one of the features of based modeling, does not require mathematical knowledge. Therefore, the description of events in the process of it is a useful method for simulation and scaling of complex adsorption systems [28,29]. Percent removal is an important parameter for the adsorption process, but due to data collection's time-consuming nature, these data are not always available. Inspired by biological neural processing, ANN can be applied to solid–liquid separation or adsorption [30–32].

In our study, we modified it with clinoptilolite, a natural zeolite, to increase the chemical and physical resistance of chitosan. We choosed clinoptilolite, a natural zeolite, as it is a cheap and readily available adsorbent for the removal of Methylene violet (MV). We conducted MV removal from the water solutions by covering clinoptilolite with chitosan, a natural polymer to demonstrate its absorbency feature. To better understand the adsorption mechanism, the adsorbent before and after adsorption was characterized by Brunauer–Emmett–Teller (BET), X-ray diffraction (XRD), and scanning electron microscopy (SEM)/energy-dispersive X-ray spectroscopy techniques. The effects of the important parameters such as pH, contact time, initial MV concentration, temperature and adsorbent dose were examined. Also adsorption equilibrium data Langmuir and Freundlich adsorption models it has been applied. The kinetics, thermodynamic and also examined desorption studies. In addition, in order to determine the availability of MV from aqueous media, experimental five inputs (initial pH, contact time, temperature effect, initial concentration and adsorbent dose and one output (removal)) parameters were developed to account the MV effects on the adsorption of an ANN model.

2. Experiment

2.1. Materials and instruments

The clinoptilolite in this study was obtained from the Manisa/Gördes region and the MV ($C_{24}H_{28}N_3Cl$) was obtained from the company Merck (Darmstadt, Germany). The chemical structure of MV is illustrated in Fig. S2. The chemicals used in this study are 0.1 M HCl, 0.1 M NaOH for pH adjustment of the solutions, CH_3COOH, chitosan for use during the experiment and were obtained from Merck Company (Darmstadt, Germany). All the chemical substances which used in the experiments were analytically pure and were freshly prepared to use in these tests. The stock solution was prepared as 1,000 mg L^{-1}. The study solutions and standard solutions were prepared by diluting the stock solution with deionized water (chemical resistance: 18 MΩ.cm).

2.2. Preparation of chitosan-coated clinoptilolite

8.0 g of the chitosan was mixed with 2% acetic acid on a magnetic stirrer for 5 h (room temperature) until it reached a gel-like consistency was obtained. In a separate beaker,

40 g of powdered clinoptilolite was mixed with 400 mL of the distilled water for 30 min. These solutions prepared in two separate cups then they were assembled in a standard single cup and then it was mixed in the magnetic agitator at room temperature for 1.5 h. After agitation, adjusted the pH value was adjusted to 6 with a 2 mol L^{-1} NaOH solution. The resulting particles were subjected to a 24-hour NaOH bath. After the resulting composites were filtered, the composite beads were then subjected to drying in for 60°C–70°C.

2.3. Characterization

The surface area of the adsorbent was determined using the BET method (Micromeritics USA, ASAP 2020). The SEM analyses were achieved under high vacuum and at 20 kV in a JEOL JSM-6060LV device. For this purpose, firstly, the gold coating was applied to the powdered samples to ensure conductivity. Subsequently, images detected by using the scanning electron microscope, in a resolution of 50 μm 200 nm and with an enlargement ratio of 1.000x–300,000x. In the quantitative structural analysis of these produced samples, an X-ray diffractometer (XRD) device which the brand name Rigaku was used. The sample was analyzed at positions between 10° and 80° 2θ angles.

2.4. Adsorption experiments

The stock MV solution was prepared with distilled water at a concentration of 1,000 mg L^{-1}. In pH adjustments, either 0.1 M NaOH or 0.1 M HCl was used. Chitosan-coated zeolite (CCZ) beads of 0.1 g/100 mL were added to the solutions and stirred in the agitator at a speed of 250 rpm. The calibration curve it was obtained by making a standard solution from the stock MV solution. The prepared standards were then analyzed on a UV-Vis spectrophotometer at λ_{max} 572 nm.

In adsorption tests, the influence of the following parameters were determined separately: pH values (2–9), contact time (5–120 min), initial dye concentration (25–125 mg L^{-1}), adsorbent dosage (0.1–1.0 g) and treatment temperature (298–318 K). When the system reaches equilibrium during the adsorption process, the amount of substance that the adsorbent substance adsorbs is a function of temperature, concentration, pressure, or equilibrium pressure. The adsorption efficiencies of composites were calculated according to Eqs. (1) and (2).

$$q_e = \frac{\left(C_o - C_e\right)}{m} \times V \tag{1}$$

$$\%\text{Adsorption} = \frac{\left(C_o - C_e\right)}{C_o} \times 100 \tag{2}$$

where q_e = adsorption capacity of the adsorbent (mg g^{-1}), C_o = initial MV concentration (mg L^{-1}), C_e = concentration of MV at equilibrium state (remaining without being adsorbed) (mg L^{-1}), V = volume of solution (L), m = mass of adsorbent (g).

2.5. Desorption experiments

Desorption studies were carried out to determine 0.1 g of adsorbent was mixed with dye solutions (25 mg L^{-1}, pH 7.0) in the magnetic agitator for 60 min at a rate of 250 rpm the recyclability performed of the adsorbent. Dyestuff detection tests were used to the obtained filtrate using the UV spectroscopic method. Then, the remaining substantial part was soaked in 0.1–0.3 M 50 mL NaOH for 60 min and, thus, the desorption study was carried out [33]. Before each desorption cycle, MV adsorption yield (%) was determined as mentioned down. The desorption rate is calculated in Eq. (3).

$$\%D = \frac{C_d}{C_a} \times 100 \tag{3}$$

where D% = desorption ratio, C_a = equilibrium concentration of MV during adsorption process (mg L^{-1}), C_d = equilibrium concentration of MV during desorption process (mg L^{-1}).

2.6. Modeling studies with artificial neural networks

ANN models were developed by examining the effects of some experimental parameters (initial dye concentration, initial pH, temperature, adsorbent amount and, contact time) on MV adsorption from an aqueous solution with CCZ. Created the number of processing elements in the input and output layers of the developed ANN model was depending on the geometry of the problem. In the input layer of the ANN model developed for the MV adsorption experiments, there are five processing elements containing information on adsorbate concentration, initial pH, temperature, adsorbent amount and, contact time, and one processing element containing data on percentage adsorption in the output layer. In the literature, the hidden layer and the number of processing elements in these layers are determined by the trial-and-error method [34]. There is no rule for determining the number of hidden layers and the number of transactions in hidden layers. In this study, the toolbox Neural Fitting Tool in MATLAB version 2008a used to create the ANN model uses one hidden layer, and can changed the number of neurons in this hidden layer. The trial-and-error method used in the literature was used to determine the number of neurons. The sigmoid transfer function (tang) is used in the hidden layer, and the linear transfer function (purely) is used in the output layer. The input matrix [G] and output vector {C} are formed from the data obtained from the experiments. The input and output data are introduced to the network using the normalization technique. Eq. (4) is used in scaling (normalizing) inputs and outputs.

$$A_i = 0.8\left[\frac{X_i - \min\left(X_i\right)}{\max\left(X_i\right) - \min\left(X_i\right)}\right] + 0.1 \tag{4}$$

where $\min(X_i)$ and $\max(X_i)$ are minimum and maximum actual experimental data.

77 data were used for the development of the ANN model. Did modeling with the hidden ANN model based on

five different input layers and single output layers known as neurons. All data were randomly divided into three categories, learning (51%), validation (15%), and testing (7%). The learning data set was used to train the ANN model. The test data set was used to evaluate the predictive capabilities of the ANN model. The result of the ANN model was evaluated using the performance criteria. The result of the ANN model is the mean square error (MSE) and the coefficient of determination (R^2). Adsorbent amount, temperature, initial pH, initial dye concentration, contact time, which are the input variables to the feed-forward neural network, are given in Table 1, which shows the working range in which the adsorption studies were carried out.

Table 1
Variable ranges of ANN model developed for MV adsorption on CCZ

Variables	Spacing
Input layer	
Adsorbent amount (g L^{-1})	(0.1–1.0)
Initial MV concentration (mg L^{-1})	(25–125)
Initial pH	(2–9)
Temperature (K)	(298–318)
Contact time (min)	(5–120)
Output layer	
MV removal (%)	(68.87–99.42)

3. Results and discussion

3.1. Textural, chemical and morphological characterization results

To examine the surface morphology, chitosan-coated clinoptilolite zeolite was subjected to the SEM before and after the adsorption process. Surface morphology, particle shape, and particle size are shown in SEM images in Fig. 1. In Figs. 1a and b, SEM images of the surface structures of clinoptilolite and chitosan are seen, respectively. SEM images of chitosan-coated clinoptilolite nanoparticles before and after the adsorption process are shown in Figs. 1c and d, respectively. The porous structure of the particles can easily seen in the zoomed images of the raw material, chitosan, before and after MV adsorption.

The porous and irregular structures seen in the SEM photos in Fig. 1 that belong to clinoptilolite. Similar results have been found in studies in the literature [13]. When the SEM images of chitosan in Fig. 1b are examined, the cross is clear that it has a homogeneous-polymer structure, although their bonding is visible. Fig. 1c shows SEM photographs of CCZ before adsorption. Fig. 1c shows that the CCZ composite has a smooth but irregular surface morphology and a porous structure [35]. When the SEM images of CCZ after MV adsorption in Fig. 1d are investigated, it is seen that MV clutches to the porous surface of CCZ and on the inner side of the particles, which shows that the adsorption process was successfully accomplished.

In Figs. 2a–d diffraction patterns of crystal structures of powdered clinoptilolite, chitosan, CCZ before MV

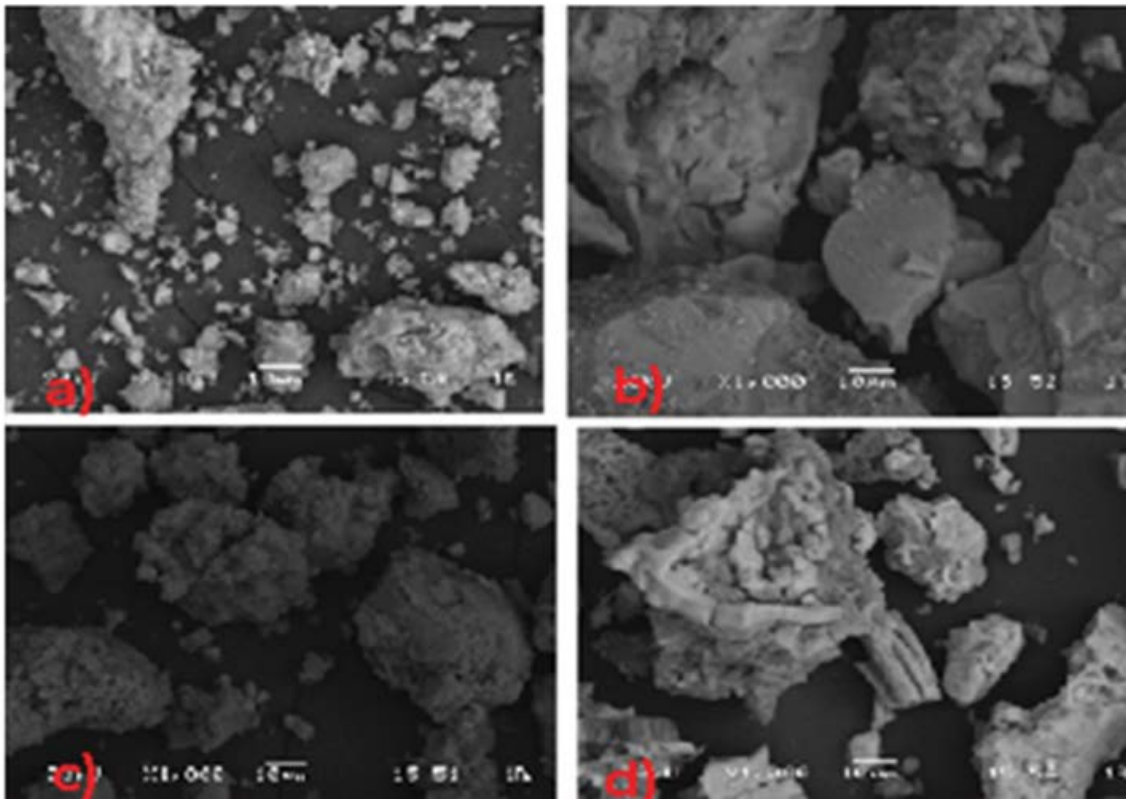

Fig. 1. SEM photographs of (a) clinoptilolite, (b) chitosan, (c) CCZ before MV adsorption, and (d) CCZ after MV adsorption.

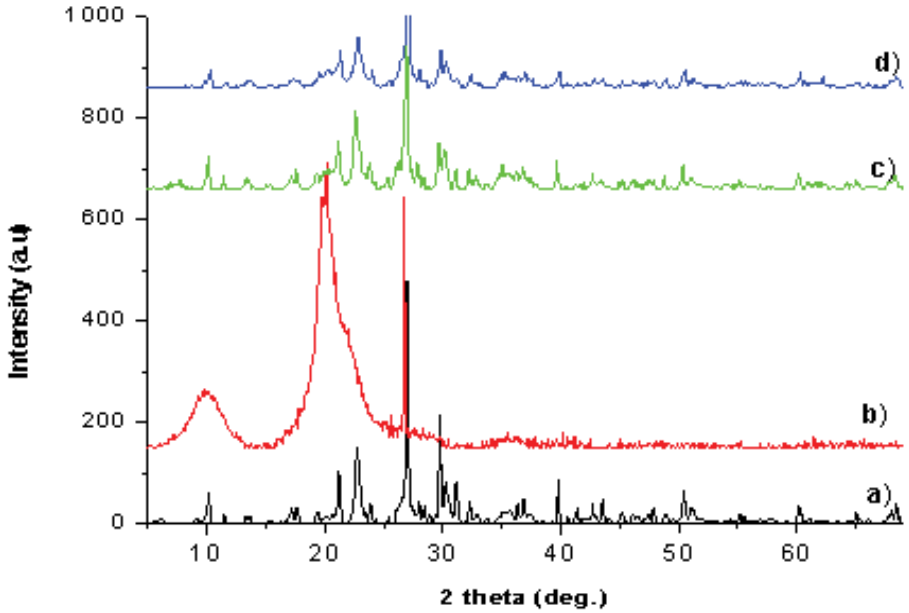

Fig. 2. XRD patterns of (a) clinoptilolite, (b) chitosan, (c) CCZ before MV adsorption, and (d) CCZ after MV adsorption.

adsorption and CCZ after adsorption are shown by the XRD spectrum.

When the XRD spectrum of the clinoptilolite is analyzed in Fig. 2, it is seen that the clinoptilolite contains sharp peaks. In Fig. 2a, characteristic 2θ reflection peaks of clinoptilolite were observed at 10.19°, 22.74°, 26.96°, and 31.12°. These sharp peaks denote that clinoptilolite has a high crystallinity structure which is supported by the results in the literature [36,37]. Fig. 2b shows that the characteristic 2θ reflection peaks of chitosan were observed at 9.88°, 20.03°, and 26.73°. These blunt peaks show us the amorphous nature of chitosan. Similar results are available in various studies in the literature [38]. As seen in Fig. 2c, the characteristic 2θ reflection peaks of CCZ before adsorption are typical refraction peaks for chitosan, such as 10.15°, 22°, 22.56°, 26.90°, 10° and 20°. These peaks show that, the peak values increased with the combination of clinoptilolite and chitosan within CCZ, and it contains an amorphous structure. When this situation is analyzed, it is observed that it does not appear to show any characteristic peak after activation. The results in the literature also support this [38]. Fig. 2d shows the characteristic 2θ reflection peaks of the dye bearing CCZ as 10.30°, 22.84°, 27.06°, 30.28°, 10°, 20° and 30° are the breakage peaks for chitosan and clinoptilolite. These observed peaks show that, with the combination of clinoptilolite and chitosan within the CCZ, the peak values increase presenting an amorphous structure. When this situation is analyzed, it is observed not to show any characteristic peak after activation. The results in the literature also support this case [37–39].

The surface area of the adsorbent is effective in the adsorption process [40–43]. The higher the surface area of the adsorbent, the higher is the adsorption. As seen in Table S1, while the BET surface area of clinoptilolite was 0.469 $m^2 g^{-1}$ in our study, it was found to be 13.010 $m^2 g^{-1}$ when coated with chitosan. Since the increase in the BET surface area will cause an increase in the adsorption capacity, we think that the use of chitosan in our study is positive.

3.2. Effects of pH and adsorbent dosage

One of the most critical factors that affect adsorption is pH value. Since hydrogen (H^+) and hydroxyl (OH^-) ions are strongly adsorbed, the adsorption of other ions affect the pH of the solution. It not only affects the ionization degree of the adsorbents but also affects their surface loads [44]. In order to investigate the effect of pH over the adsorption of MV onto CCZ, MV solutions with a concentration of 100 mg L^{-1} were prepared at varying pH values (2–9). The data obtained on the effect of the initial pH value on MV adsorption and the changing pH value on against the changes in the adsorption are shown in the graph in Fig. 3a. In order to determine adsorbent dosage in dye adsorption, it was studied between adsorbent concentrations of 0.1 and 0.2 g L^{-1}.

3.3. Effect of the contact time

The properties of the sorption centers and the retained material have a significant effect on the time required for the adsorption to reach equilibrium [45]. The time needed for its concentration to reach equilibrium state was determined for the kinetic experiments, and the results obtained for methyl violet are given in Fig. 3b. The contact time of up to 120 min was examined for the stabilization of the adsorption.

3.4. Effect of adsorbent dosage and initial MV concentration on adsorption

In adsorption studies, the amount of adsorbent is one of the critical factors affecting the efficiency of the dye to be

adsorbed [46]. If the amount of adsorbent added is insufficient, the maximum adsorption efficiency may decrease. If the amount of adsorbent is too high, flocculation may occur in the solution. Both situations have negative effects on adsorption [47]. The experiments were done with variable initial MV concentration (25, 50, 75, and 100 mg L^{-1}), and adsorbent dose of (0.1–1.0 g/100 mL), a contact time of 60 min, a temperature of 298 K, and a stirring speed of 250 rpm.

As seen in Fig. 3a, MV adsorption increased with increasing pH value. It is assumed that this is due to possibly an excess of OH^- ions in the area and the cationic structure of the dye. At basic pHs, it is thought that the excess OH^- ion in the field forms a complex with the cationic dye, thus decreasing the adsorption [45]. Under conditions of pH ≥ 6, MV adsorption is much higher than at acidic pHs.

According to the results obtained from the experiments in Fig. 3b, the adsorption first increased with an increasing time. After reaching the equilibrium after a while, the dye retention rate has fixed.

Fig. 3c, MV removal increases with increasing concentration and amount of adsorbent. Since there was no significant increase in all concentrations among the amount, the adsorbent amount was considered to be 0.1 g as optimum. These results show us that the dye adsorption is related to the initial concentration. As the highest adsorption capacity was observed at 100 mg L^{-1} initial concentration, the initial concentration was taken as 100 mg L^{-1} in the following thermodynamic and kinetics studies.

3.5. Adsorption isotherms

For the purpose of determining the conformity of these obtained data to the isotherm model, the relation between equilibrium concentration and C_e/q_e should be examined. Equal amounts of samples were analyzed at 579 nm with a UV-Vis spectrophotometer. Using the data obtained from different initial concentration studies, how the adsorption changes was investigated by using Langmuir and Freundlich adsorption isotherms (Figs. 4a and b). This relationship is described with the use of the equation and curve formation given in Eqs. (5) and (6). The isotherm constants are then obtained by the curve and shift values.

$$\frac{C_e}{q_e} = \frac{1}{q_m K_L} + \frac{1}{q_m} C_e \tag{5}$$

$$\ln q_e = \ln K_f + \frac{1}{n} \ln C_e \tag{6}$$

where q_e = the adsorbed amount at equilibrium (mg g^{-1}), C_e = concentration of the adsorbate in solution at equilibrium (mg L^{-1}). q_{max} = maximum adsorption capacity (mg g^{-1}), K_L (L mg^{-1}) = the Langmuir constant [48]; K_f (L g^{-1}) = a constant regarded with the adsorption capacity, $1/n$ = a model parameter involving the adsorption intensity. The analysis of the adsorption data in the event of achieving equilibrium is important for the optimization of the adsorption process. With this aim, how the adsorption changed was examined using different forms of adsorption isotherm (Langmuir and Freundlich isotherms) by using different data obtained in the different studies. The suitability of the Langmuir isotherm for the experimental data was determined by the high correlation value (R^2 = 0.99). This relation was delineated with the equation and plots given in Fig. 5a and then isotherm constants were derived from the slope and shift values. The analysis of adsorption data at the state of equilibrium is important for optimizing of the adsorption process.

The regression numbers (R^2) and coefficients of isotherm the models were calculated with the help of linear lines. The results obtained for three different temperatures are given in Table S2.

Table S2 shows that, as a consequence of calculations made regarding MV adsorption, for CCZ, the q_{max} value for three different temperatures (298–318 K) was found to be 56.82, 104.17 and 111.11 mg g^{-1} respectively. As it can be seen from Table S2, the value of q_{max} increased as the temperature increased. The isotherms obtained at various temperatures for MV adsorption have been demonstrated by Langmuir and Freundlich models. When the correlation coefficients of both models were compared, it was seen that the CCZ samples produced fit the Langmuir isotherm. It was determined that the highest value of q_{max} was 318 K.

3.6. Adsorption kinetics

Adsorption kinetics is employed to determine which mechanisms play a role during the adsorption of the adsorbed substance on the adsorbent surface. Adsorption kinetics may well be defined with pseudo-first and second-order equations [49]. The pseudo-first, and second-order equations are given below, respectively [Eqs. (7) and (8)]:

3.6.1. Pseudo-first-order equation

$$\ln\left(q_e - q_t\right) = \ln q_e - k_1 t \tag{7}$$

where q_e = amount of adsorbed substance per gram of adsorbent at equilibrium state (mg g^{-1}); q_t = amount of adsorbed substance per gram of adsorbent at any time (mg g^{-1}); t = contact time (min); k_1 = rate constant of the pseudo-first-order (min^{-1}).

3.6.2. Pseudo-second-order equation

The linearity of the kinetic model is of high importance in the determination of the model that best fits the adsorption system.

$$\frac{t}{q_t} = \frac{1}{k_2 q_e^2} + \frac{t}{q_e} \tag{8}$$

where k_2 = pseudo-second-order equation constant (g mg^{-1} min^{-1}); t = determined time constant (min); q_t = amount of adsorbed substance at the end of time (mg g^{-1}); q_e = amount of adsorbed substance at equilibrium (mg g^{-1}) [50].

The obtained q_e calculated velocity constants and correlation coefficients are all given in Table S3.

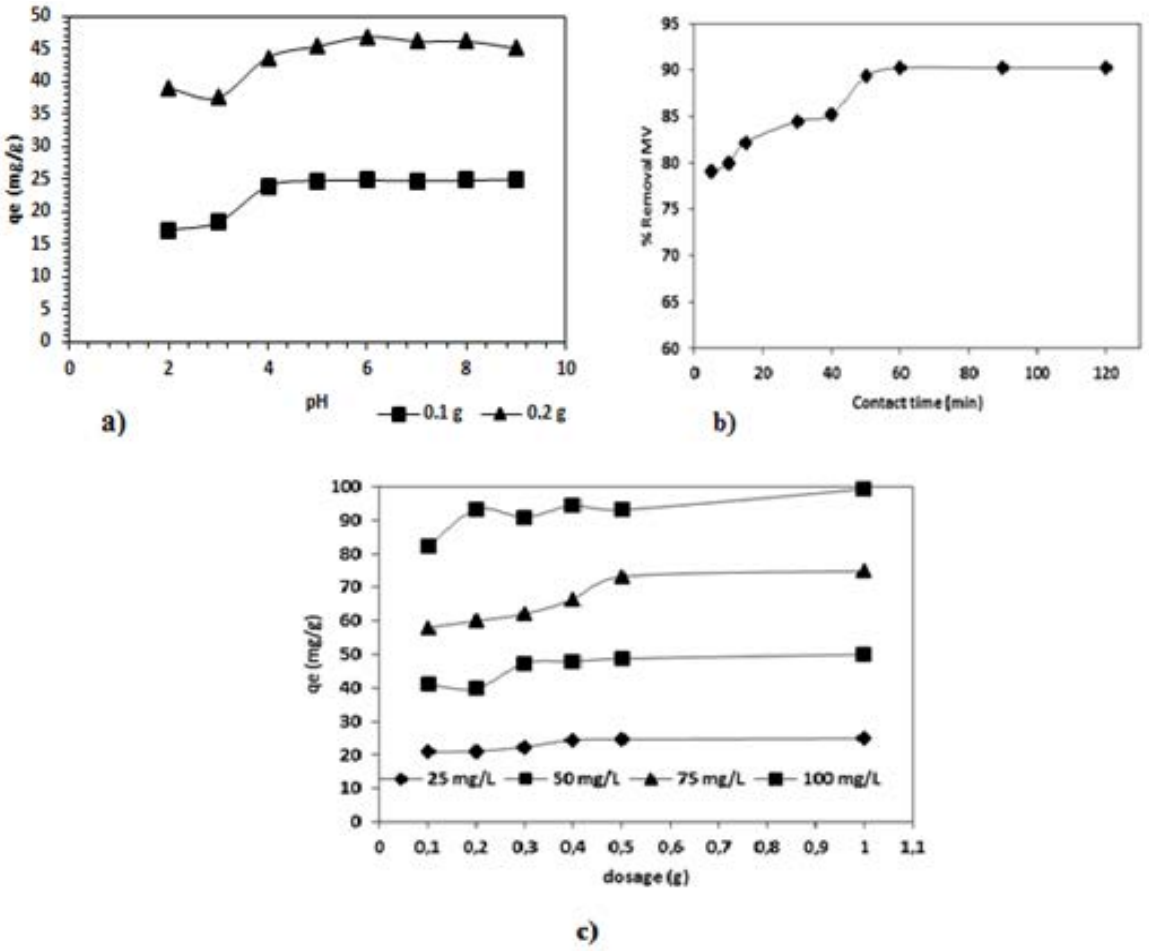

Fig. 3. (a) The pH influence on the adsorption, (b) effect of mixing time on the adsorption and (c) effect of adsorbent dosage on the adsorption.

Although the R^2 value in the first-order equation is considerably smaller than 1, the R^2 value of the second-order equation is bigger than 0.99 and close to 1 (Fig. 5). In addition, the amount of MV removed per adsorbent is higher in the second-order equation compared to the first, so it is concluded that the kinetic data conformed more to the second-degree kinetic model. Similar approaches have been achieved in several studies made in the literature for the adsorption of dyestuffs [50–52].

3.7. Thermodynamics parameters of the adsorption

The influence of the temperature on the MV adsorption on CCZ was studied in the range of 298–318 K. By using 0.1 g of CCZ and MV solutions at a concentration of 100 mg L^{-1}, the effect of temperature on MV adsorption was studied. The thermodynamic parameters of MV adsorption were determined from the experimental results obtained at different temperatures using Eq. (9):

T (K) is the solution temperature.

The standard enthalpy $\Delta H°$ and entropy $\Delta S°$ can be determined from the following van't Hoff Eqs. (10) and (11).

$$\Delta G° = -RT \ln K_L \tag{9}$$

$$\ln K_L = \frac{q_e}{C_e} \tag{10}$$

According to the van't Hoff equation:

$$\ln K_L = \frac{\Delta S°}{R} - \frac{\Delta H°}{RT} \tag{11}$$

where K_L = distribution coefficient, q_e (mg g^{-1}) = adsorption capacity at equilibrium, C_e (mg L^{-1}) = MV concentration at equilibrium and R = universal gas constant.

The thermodynamic parameters obtained for MV adsorption are given in Table S4. These adsorption data show that $\Delta G°$ is negative at all temperatures which verify the spontaneous nature of adsorption. If $\Delta H°$ is positive, it shows that the adsorption process is endothermic. In other words, the applicability of the adsorption process can be comprehended with a negative Gibbs free energy and enthalpy value. The positively yielding $\Delta S°$ values show the

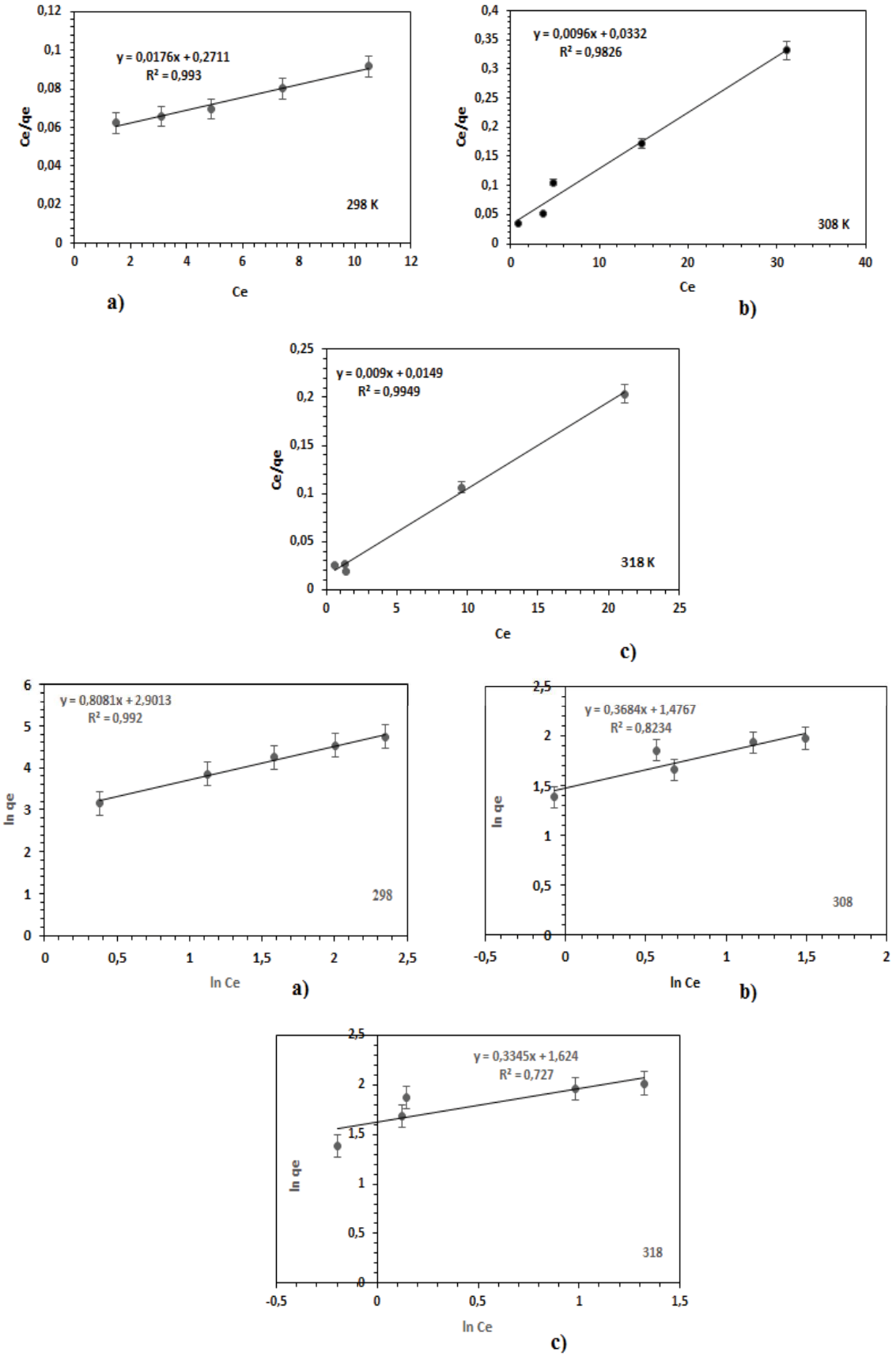

Fig. 4. (a) Langmuir isotherm plots obtained for the adsorption MV onto CCZ sorbent (pH: 7, contact time: 60 min, adsorbent dose: 0.1 g). (b) Freundlich isotherm plots obtained for the adsorption MV onto CCZ.

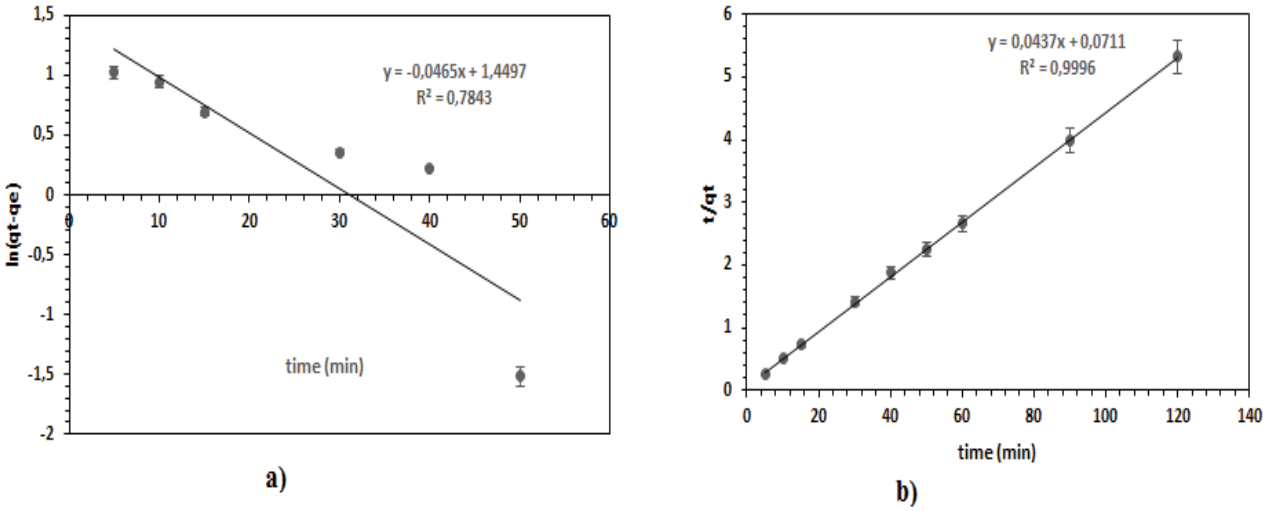

Fig. 5. (a) Pseudo-first-order and (b) pseudo-second-order kinetic plots for adsorption of MV onto CCZ.

Table 2
Comparison of MV adsorption among different adsorbents

Adsorbent	pH	Temperature (K)	Adsorption capacity (mg g^{-1})	Reference
Banana peel	6–7	303	7.90	[62]
Orange peel	7	303	6.10	[62]
Sepiolite	6–7	333	10.24	[58]
Bagasse fly ash	6	303	26.25	[59]
Mansonia sawdust	10	299	16.11	[60]
HNT-Fe_3O_4	7	303	20.04	[61]
Carbon covered sand	7	298	49.03	[63]
CCZ	6	318	111.11	This study

increased randomness of the adsorbent on the solid–liquid interface [51–54]. As the temperature increases, MV adsorption also increases, and that shows us that the MV adsorption process is endothermic.

The distinctiveness of the adsorption process depends on the Gibbs free energy, and the calculation of the negative $\Delta G°$ value suggests that adsorption occurs spontaneously [44,55–57]. Besides, the increment in $\Delta G°$ with the increasing temperature shows that MV is better adsorbed at higher temperatures. The positive value of $\Delta H°$ is indicative of the endothermic character of adsorption. Standard entropy values, on the other hand ($\Delta S°$), were found positive for all temperature values. The positive value of $\Delta S°$ denotes that a structural change is possible between the adsorbent and the dyestuff.

3.8. Comparison of adsorption capacity of the developed CCZ for MV removal

In Table 2, the maximum MV adsorption capacities are summarized in case diverse adsorbents are used [58–63].

As seen from Table 3, the high adsorption capacity obtained in the study with chitosan-coated zeolite is observed to be a satisfactory method for MV removal compared to other different adsorbents CCZ. This result shows that the adsorbent CCZ has an effective adsorption capacity in removing MV from aqueous solutions and can be used as a suitable adsorbent in wastewater treatment.

3.9. Regeneration of adsorbents

The desorption and recyclability options were investigated. A high desorption rate of a bio adsorbent is a desired property for an adsorbent. As it will decrease of the adsorbent consumption, costs will also drop. In the performed adsorption–desorption tests, the results obtained from seven adsorption–desorption cycles for the adsorbed MV are given in Fig. S3.

Fig. S3 shows the CCZ recycle performance graph. In order to recover the MV that has clung onto CCZ and to understand the adsorption mechanism, desorption studies were achieved with 0.1 g of CCZ and 0.05, 0.1, and 0.2 M NaOH solutions. Recycling rates dropped from 80% to 62% gradually, whereas no decrease was observed during the adsorption cycles. However, in the first and seventh desorption cycles, a decrease of 18% was seen. This shows that CCZ is a suitable adsorbent from the aspect of recycling.

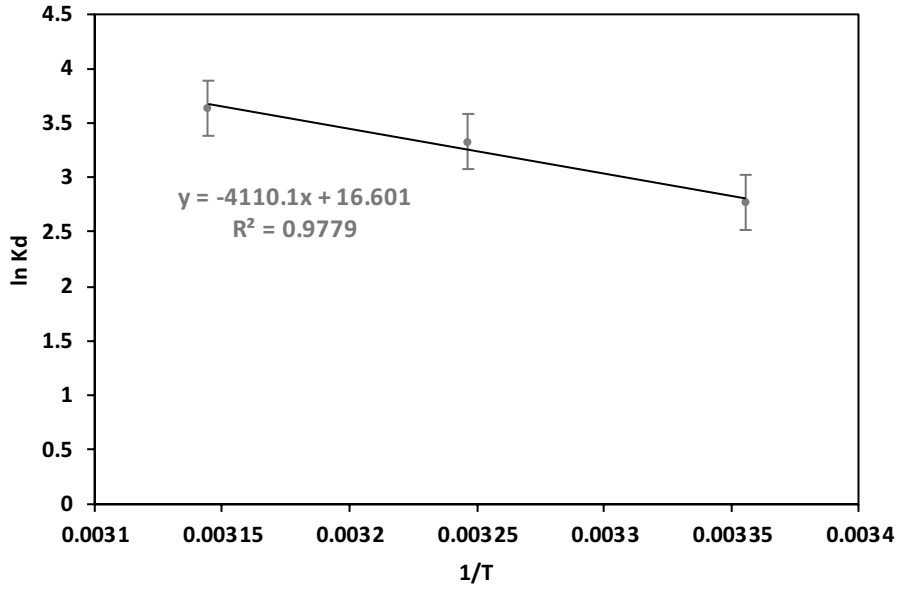

Fig. 6. lnK_d vs. 1/T graph.

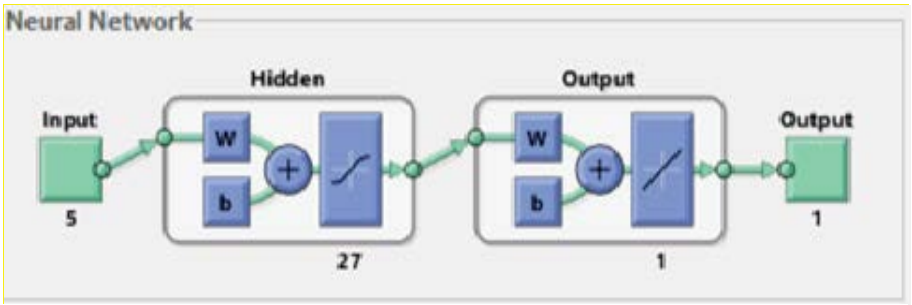

Fig. 7. Optimum ANN structure (5-20-1).

3.10. Modeling of MV adsorption on CCZ with ANN

In the study, the initial pH, initial dye height, temperature, contact time, and initial adsorbent amount were defined as input data for the ANN system for the adsorption system, while the dye removal value in the output layer was estimated. In the ANN training of the adsorption system where MV removal was examined, the experimental data were divided into 51% training, 15% validation, and 7% test. The maximum epoch value is determined as 12,000 iterations. To determine the optimal architecture of the ANN model, maximum the R^2 value of the test dataset is used. Realized using the training process standard back-propagation an algorithm as optimization procedure. The optimal topology for the adsorption of MV on CCZ was determined as 5-20-1 with R^2 and MSE values (Fig. 7).

The graphics obtained for the biosorption system with ANN are presented in Fig. 7. *R*-value is available on the graphs with experimental and predicted data. R^2 value is a statistical method used to measure the relationship of a variable with two or more variables or the linear relationship or degree between two variables. Neurons were used in the hidden layer and were determined by the trial and error method according to the obtained R^2 value. After the input variables are defined as entering the system, the graph given by the program is presented in Fig. 8.

When Fig. 8 is examined, the graphs consist of three indicators: data, fit, and $Y = T$. While there are experimental data used in network training on the x-axis, there are estimated values on the y-axis. The relationship between the input, and the estimated value is shown by the line of feet. The $Y = T$ line is the true value and the estimated value is equal, that is, the targeted line. The data are the model estimation values obtained by ANN. The correlation from training data for the ANN model optimized structure is shown in Fig. 8a. As can be seen in Figs. 8b and c, it performed relatively well in verification and testing, although it was distributed in some data. The regression coefficient for training, validation and testing steps was determined as 94% for training, 88% for validation and 93% for testing. The optimal tapology for the adsorption of MV onto CCZ was determined with R^2 and MSE values of 0.93 and 0.064, respectively. With the obtained high correlation coefficient, and the complex relationship between ANN input and output, the number of hidden layers and the number of processing elements in the hidden layer, the network architecture was determined by taking the closest output to

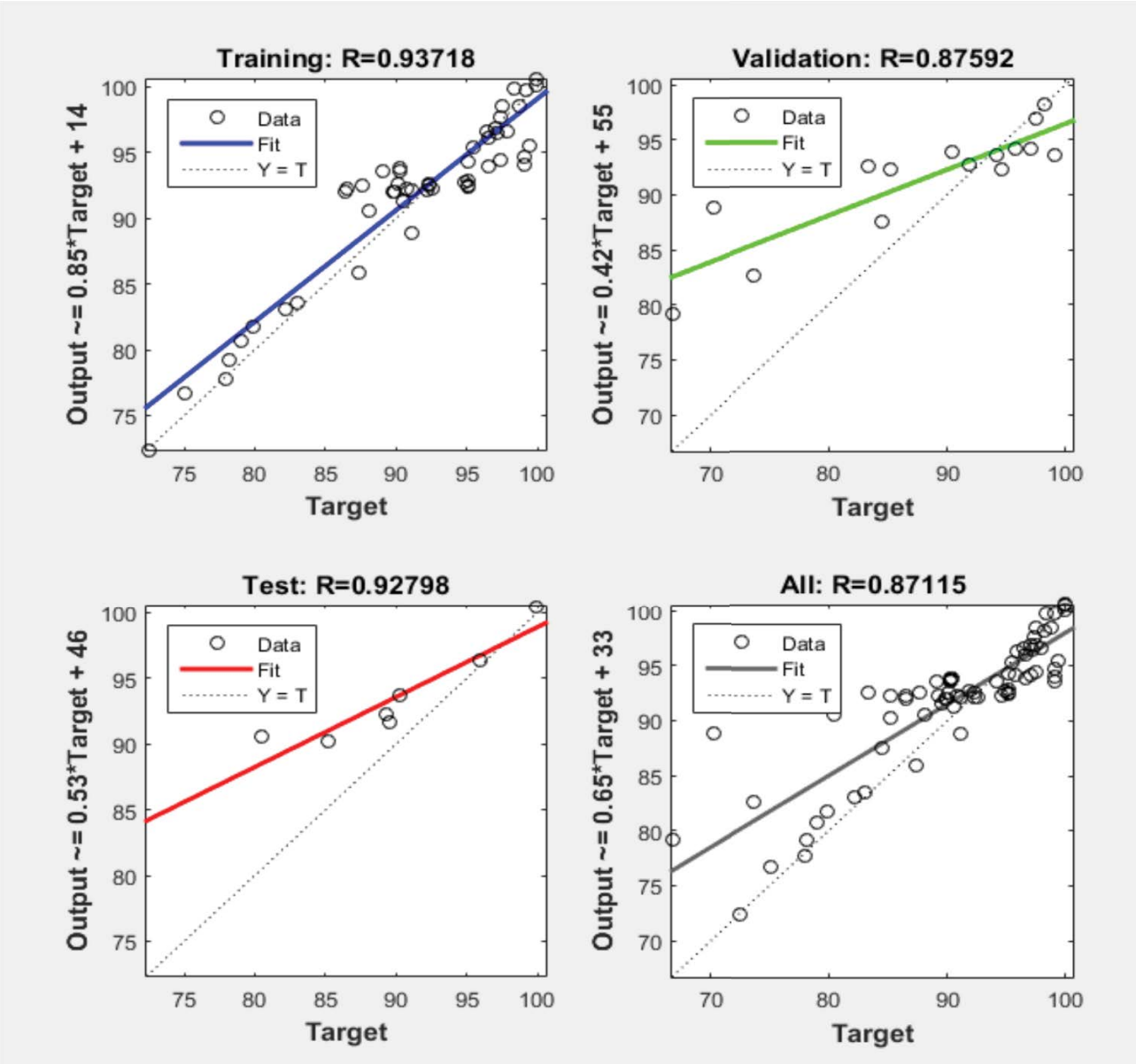

Fig. 8. ANN predictive model graph.

the desired values and the relationship between input–output variables were defined, and high accuracy estimation was obtained.

4. Conclusions

Clinoptilolite and chitosan are reasonably suitable materials due to their large surface areas for MV dye to cling onto. The largest BET surface area is found to be 13.00 $m^2 g^{-1}$ in CCZ. Since CCZ is a porous composite structure, it yields successful results in adsorption. The obtained CCZ adsorbent was used effectively to remove the MV dyestuff from the aqueous solution under the optimum batch conditions, 0.1 g/100 mL of adsorbent dosage, pH 7, and contact time of 60 min. The isotherms of MV adsorption obtained at different temperatures are shown through the Langmuir and Freundlich models. As a result of the calculations made regarding MV adsorption, CCZ q_{max} value (318 K) was found as 111.11 mg g^{-1}. Due to the large surface area and homogenous surface, the optimal temperature for MV adsorption with CCZ was determined as 298 K, and it was observed to be coherent with both the Langmuir and Freundlich isotherms at room temperature. In light of these findings, since CCZ samples are efficient in dye removal, they are a promising material for removing dye from discharge waters, as they are environmental-friendly, low-cost, and efficient. The ANN model was first developed using a three layer back-propagation. Network Model with 5-20-1 optimum structure used the tangent sigmoid transfer function. Input is in the hidden layer, and a linear transfer function

is used in the output layer. All these results show that there is an agreement between the experimental data and the predicted data obtained from the ANN model.

Acknowledgement

We here by thank to Academic Proofreading for language support for professional editing service for language of manuscript.

References

[1] R.V.N. Kandisa, K.V. Narayana Saibaba, K.B. Shaik, R. Gopinath, Dye removal by adsorption: a review, Bioreme. Biodegrad., 7 (2016) 1–4.
[2] H.M.S. Munir, N. Feroze, A. Ikhlaq, M. Kazmi, F. Javed, H. Mukhtar, Removal of colour and COD from paper and pulp industry wastewater by ozone and combined ozone/UV process, Desal. Water Treat., 137 (2019) 154–161.
[3] P. Kumar, R. Agnihotri, K.L. Wasewar, H. Uslu, C.K. Yoo, Status of adsorptive removal of dye from textile industry effluent, Desal. Water Treat., 50 (2012) 226–244.
[4] A. Ikhlaq, F. Javed, A. Niaz, H.M.S. Munir, F. Qi, Combined UV catalytic ozonation process on iron loaded peanut shell ash for the removal of methylene blue from aqueous solution, Desal. Water Treat., 200 (2020) 231–240.
[5] E. Altintig, S. Altundag, I. Yakan, D. Bozdag, H. Altundag, Mathematical approach to artificial neural network on methyl violet removal with magnetically coated activated carbon, Desal. Water Treat., 239 (2021) 202–216.
[6] A. Dabrowski, Adsorption, from theory to practice, Adv. Colloid Interface Sci., 93 (2001) 135–224.
[7] G. Crini, Non-conventional low-cost adsorbents for dye removal: a review, Bioresour. Technol., 97 (2006) 1061–1085.
[8] M. Toor, B. Jin, Adsorption characteristics, isotherm, kinetics, and diffusion of modified natural bentonite for removing diazo dye, Chem. Eng. J., 187 (2012) 79–88.
[9] K. Rida, S. Bouraoui, S. Hadnine, Adsorption of methylene blue from aqueous solution by kaolin and zeolite, Appl. Clay Sci., 83–84 (2013) 99–105.
[10] L. Wang, J. Zhang, R. Zhao, Adsorption of basic dyes on activated carbon prepared from *Polygonum orientale Linn*: equilibrium, kinetic and thermodynamic studies, Desalination, 254 (2010) 68–74.
[11] S. Malamis, E. Katsoua, A review on zinc and nickel adsorption on natural and modified zeolite, bentonite and vermiculite: examination of process parameters, kinetics and isotherms, J. Hazard. Mater., 252–253 (2013) 428–461.
[12] V.V. Panic, S.J. Velickovic, Removal of model cationic dye by adsorption onto poly(methacrylic acid)/zeolite hydrogel composites: kinetics, equilibrium study and image analysis, Sep. Purif. Technol., 122 (2014) 384–394.
[13] Z. Dikmen, O. Orhun, Preparation of magnetic modified synthetic and natural zeolites and comparison of some of their physical characteristics, Anadolu Univ. J. Sci. Technol. Appl. Sci. Eng., 14 (2013) 75–90.
[14] M.D. Lenardon, C.A. Munro, N.A.R. Gow, Chitin synthesis and fungal pathogenesis, Curr. Opin. Microbiol., 13 (2010) 416–423.
[15] M. Vakili, M. Rafatullah, B. Salamatinia, Application of chitosan and its derivatives as adsorbents for dye removal from water and wastewater, Carbohydr. Polym., 113 (2014) 115–130.
[16] F. Croisier, C. Jérôme, Chitosan-based biomaterials for tissue engineering, Eur. Polym. J., 49 (2013) 780–792.
[17] N. Shaari, S.K.J. Kamarudin, Chitosan and alginate types of bio-membrane in fuel cell application: an overview, Power Sources, 289 (2015) 71–80.
[18] Z. Bekci, C. Ozveri, S. Yoldas, K. Yurdakoc, Sorption of malachite green on chitosan bead, J. Hazard. Mater., 154 (2008) 254–261.
[19] W.S.W. Ngah, L.C. Teong, M.A.K.M. Hanafiah, Adsorption dyes and heavy metal ions by chitosan composites, Carbohydr. Polym., 83 (2011) 1446–1456.
[20] D. Kołodynska, P. Hałas, M. Franus, Z.J. Hubicki, Zeolite properties improvement by chitosan modification—sorption studies, Ind. Eng. Chem., 52 (2017) 187–196.
[21] W.A. Khanday, M. Asif, B.H. Hameed, Cross-linked beads of activated oil palm ash zeolite/chitosan composite as a bio-adsorbent for the removal of methylene blue and acid blue, 29 dyes, Int. J. Biol. Macromol., 95 (2017) 895–902.
[22] S.K. Alpat, O. Ozbayrak, S. Alpat, H.J. Akcay, The adsorption kinetics and removal of cationic dye, Toluidine Blue O from aqueous solution with Turkish zeolite, J. Hazard. Mater., 151 (2008) 213–220.
[23] D. Baybas, U.J. Ulusoy, Polyacrylamide-clinoptilolite/Y-zeolite composites: characterization and adsorptive features for terbium, J. Mater., 187 (2011) 241–249.
[24] P. Li, Y.J. Su, Y. Wang, B. Liu, L.M. Sun, Bioadsorption of methyl violet from aqueous solution onto Pu-erh tea powder, J. Hazard. Mater., 179 (2010) 43–48.
[25] C.H. Zhou, An overview on strategies towards clay-based designer catalysts for green and sustainable catalysis, Appl. Clay Sci., 53 (2011) 87–96.
[26] R. Celis, M.A. Adelino, M.C. Hermosín, J. Cornejo, Montmorillonite–chitosan bionanocomposites as adsorbents of the herbicide clopyralid in aqueous solution and soil/water suspensions, J. Hazard. Mater., 209 (2012) 67–76.
[27] D. Salari, N. Daneshvar, F. Aghazadeh, A.R. Khataee, Application of artificial neural networks for modeling of the treatment of wastewater contaminated with methyl tertbutyl ether (MTBE) by UV/H_2O_2 process, J. Hazard. Mater., 125 (2005) 205–210.
[28] A. Aleboyeh, M.B. Kasiri, M.E. Olya, H. Aleboyeh, Prediction of azo dye decolorization by UV/H_2O_2 using artificial neural networks, Dyes Pigm., 77 (2008) 288–294.
[29] N.G. Turan, B. Mesci, O. Ozgonenel, Artificial neural network (ANN) approach for modeling Zn(II) adsorption from leachate using a new biosorbent, Chem. Eng. J., 173 (2011) 98–105.
[30] S. Chowdhury, P.D. Saha, Artificial neural network (ANN) modeling of adsorption of methylene blue by NaOH-modified rice husk in a fixed-bed column system, Environ. Sci. Pollut. Res., 20 (2013) 1050–1058.
[31] B. Singha, N. Bar, S.K. Das, The use of artificial neural network (ANN) for modeling of Pb(II) adsorption in batch process, J. Mol. Liq., 211 (2015) 228–232.
[32] G. Wang, L. Yang, L. Jiang, Simple combination of humic acid with biogenic hydroxyapatite achieved highly efficient removal of methylene blue from aqueous solution, RSC Adv., 6 (2016) 67888–67897.
[33] Y. Zhan, J. Lin, Adsorption of humic acid from aqueous solution onto unmodified and surfactant-modified chitosan/zeolite composites, Chem. Eng. J., 200–202 (2012) 202–213.
[34] Z.U. Ahmad, L. Yao, Q. Lian, F. Islam, M.R. Zappi, D.D. Gang, The use of rtifical neural network (ANN) for modeling adsorption of sunset yellow onto neodymium modified ordered mesaporous carbon, Chemosphere, 256 (2020) 1–16.
[35] K. Yang, X. Zhang, C. Chao, B. Zhang, L. Jindun, In-situ preparation of NaA zeolite/chitosan porous hybrid beads for removal of ammonium from aqueous solution, Carbohydr. Polym., 107 (2014) 103–109.
[36] N. Ajoudanian, A. Nezamzadeh-Ejhieh, Enhanced photocatalytic activity of nickel oxide supported on clinoptilolite nanoparticles for the photodegration of aqueous cephalexin, Mater. Sci. Semicond. Process., 36 (2015) 162–169.
[37] M. Nairat, T. Shahwan, A.E. Eroglu, H. Fuchs, Incorporation of iron nanoparticles into clinoptilolite and its application for the removal of cationic and anionic dyes, J. Ind. Eng. Chem., 21 (2015) 1143–1151.
[38] R.S.C.M. Queiroz Antonino, B.R.P.L. Fook, V.A.O. Lima, R.Í. Farias Rached, E.P.N. Lima, R.J. Silva Lima, C.A.P. Covas, M.V. Lia Fook, Preparation and characterization of chitosan obtained from shells of shrimp (*Litopenaeus vannamei* Boone), Mar. Drugs, 15 (2017) 1–12.
[39] W.A. Khanday, S.A. Majid, S.C. Shekar, R. Tomar, Dynamic adsorption of DMMP over synthetic zeolite-Alpha, Arabian J. Chem., 7 (2014) 115–123.

[40] E. Agus, P. Wibowo, N.R. Aji, N. Widiarti, Synthesis of TiO_2/chitosan photocatalyst, TiO_2/bentonite and adsorption of zeolite to purify Unnes's Water Reservoir, Int. J. Chemtech. Res., 10 (2017) 62–69.
[41] R. Serezli, A. Tabak, Unye bentonit ile sulu ortamdan amonyum adsorpsiyonu, Ekoloji, 22 (2013) 35–42.
[42] Z. Zhou, S. Lin, T. Yue, T.C. Lee, Adsorption of food dyes from aqueous solution nanoparticles, J. Food Eng., 126 (2014) 133–141.
[43] W. Sumarni, R.S. Iswari, P. Marwoto, E.F. Rahayu, Physical Characteristics of Chitosan-Silica Composite of Rice Husk Ash, IOP Conf. Ser.: Mater. Sci. Eng., 107 (2016) 1–9, doi: 10.1088/1757-899X/107/1/012039.
[44] L. Liu, Y. Lin, Y. Liu, Y. Zhu, Q.J. He, Removal of methylene blue from aqueous solutions by sewage sludge based granular activated carbon: adsorption equilibrium, kinetics, and thermodynamics, Chem. Eng., 58 (2013) 2248–2253.
[45] D. Lee, R.E. Cohen, M.F. Rubner, Heterostructured magnetic nanotubes, Langmuir, 23 (2007) 123–129.
[46] E. Altintig, A. Alsancak, H. Karaca, D. Angin, H. Altundag, The comparison of natural and magnetically modified zeolites as an adsorbent in methyl violet removal from aqueous solutions, Chem. Eng. Commun., (2021), doi: 10.1080/00986445.2021.1874368.
[47] X. Xiao, S. Luo, G. Zeng, W. We, Y. Wan, L. Chen, H. Gou, Z. Cao, L. Yang, J. Chen, Q. Xi, Biosorption of cadmium by endophytic fungus (EF) *Microsphaeropsis* sp. LSE10 isolated from cadmium hyperaccumulator *Solanum nigrum* L., Biosesour. Technol., 101 (2019) 1668–1674.
[48] V.M. Boddu, K. Abburi, J.L. Talbott, E.D. Smith, Removal of hexavalent chromium from wastewater using a new composite chitosan biosorbent, Environ. Sci. Technol., 37 (2003) 4449–4456.
[49] I. Ullah, R. Nadeem, M. Iqbal, Q. Manzoor, Biosorption of chromium onto native and immobilized sugarcane bagasse waste biomass, Ecol. Eng., 60 (2013) 99–107.
[50] B. Acemioglu, Removal of Fe(II) ions from aqueous solution by Calabrian pine bark wastes, Bioresour. Technol., 93 (2014) 99–102.
[51] W.A. Amer, M.A. Awwad, Removal of As(V) from aqueous solution by adsorption onto nanocrystalline kaolinite: equilibrium and thermodynamic aspects of adsorption, Environ. Nanotechnol., 9 (2018) 37–41.
[52] C. Pongener, P. Chandra, M.J. Baruah, Adsorption of fluoride onto activated carbon synthesized from *Manihot esculenta* biomass—equilibrium, kinetic and thermodynamic studies, Environ. Chem. Eng., 6 (2018) 2382–2389.
[53] H. Karaca, E. Altintig, D. Türker, M. Teker, An evaluation of coal fly ash as an adsorbent for the removal of methylene blue from aqueous solutions: kinetic and thermodynamic studies, J. Dispersion Sci. Technol., 39 (2018) 1800–1807.
[54] P.E. Kumar, M. Santhi, Adsorption of Rhodamine B from an aqueous solution: kinetic, equilibrium and thermodynamic studies, Int. J. Innov. Res. Sci. Eng. Technol., 4 (2015) 497–510.
[55] L. Cottet, C.A.P. Almedia, N. Naidek, M.F. Viante, M.C. Lopes, N.A. Debacher, Adsorption characteristics of montmorillonite clay modified with iron oxide with respect to methylene blue in aqueous media, Appl. Clay Sci., 95 (2014) 25–31.
[56] V. Javanbakht, S.M. Ghoreishi, N. Habibi, M.A. Javanbakht, Novel magnetic chitosan/clinoptilolite/magnetite nanocomposite for highly efficient removal of Pb(II) ions from aqueous solution, Powder Technol., 302 (2016) 372–383.
[57] M. Ghaedi, A. Ansari, M.H. Habibi, A.R.J. Asghari, Removal of malachite green from aqueous solution by zinc oxide nanoparticle loaded on activated carbon: kinetics and isotherm study, Ind. Eng. Chem., 20 (2014) 17–28.
[58] G. Annadurai, S.R. Juang, D.J. Lee, Use of cellulose-based wastes for adsorption of dyes from aqueous solutions, J. Hazard. Mater. B., 92 (2002) 263–274.
[59] Y. Ozdemir, M. Dogan, M. Alkan, Adsorption of cationic dyes from aqueous solutions by sepiolite, Microporous Mesoporous Mater., 96 (2006) 419–427.
[60] D.I. Mall, C.V. Srivastava, K.N. Agarwal, Removal of orange-g and methyl violet dyes bye adsorption onto bagasse fly ash kinetic study and equilibrium isotherm analyses, Dyes Pigm., 69 (2006) 210–223.
[61] A.E. Ofomaja, Kinetic study and sorption mechanism of methylene blue and methyl violet onto mansonia wood sawdust, Chem. Eng. J., 143 (2008) 85–95.
[62] L.R. Bonetto, F. Ferrarini, D.C. Marco, J.S.J. Crespo, Removal of methyl violet 2B dye from aqueous solution using a magnetic composite as an adsorbent, Water Process. Eng., 6 (2015) 11–20.
[63] S. Moradi, S. Azizian, Preparation of nanostructured carbon covered sand for removal of methyl violet from water, J. Mol. Liq., 219 (2016) 909–913.

Supplementary information

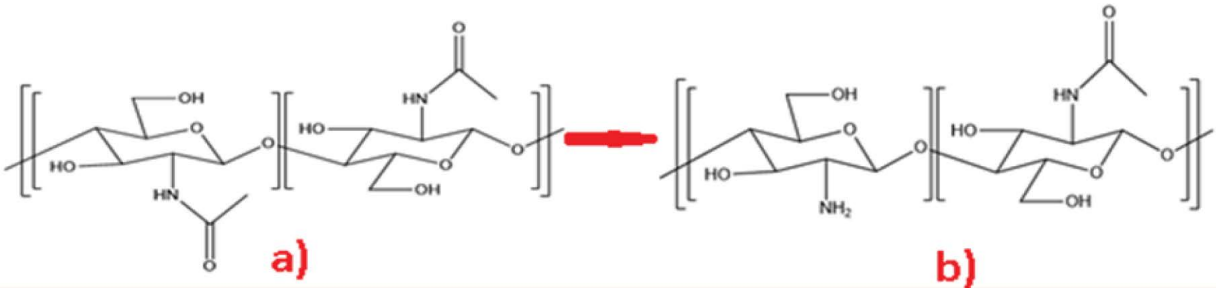

Fig. S1. Chemical structure of (a) chitin and (b) chitosan.

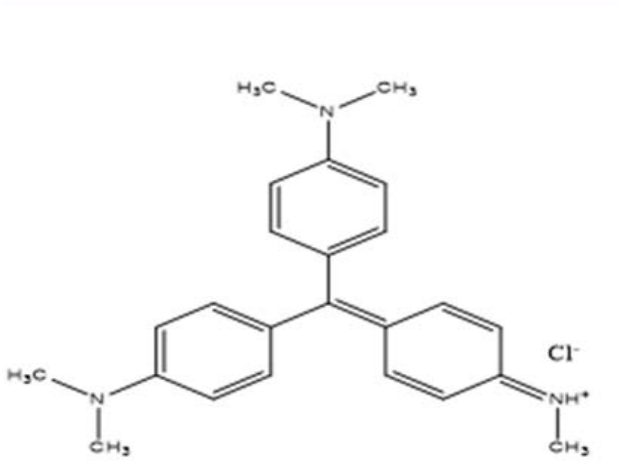

Fig. S2. Chemical structure of methyl violet.

Table S1
BET analysis results of clinoptilolite and CCZ

Textural parameter	Clinoptilolite	CCZ
BET surface area ($m^2\ g^{-1}$)	0.469	13.010
Langmuir surface area ($m^2\ g^{-1}$)	0.646	18.110
Micropore area ($m^2\ g^{-1}$)	0.558	2.678
Barrett–Joyner–Halenda average pore width (4V/A) nm	2.953	2.905
t-plot external surface area ($m^2\ g^{-1}$)	0.089	10.331

Table S2
Constants of Freundlich and Langmuir isotherms for MV adsorption on CCZ

Temperature (K)	Langmuir isotherms			Freundlich isotherms		
	q_m, (mg g^{-1})	b (L mg^{-1})	R^2	K_f	n (L mg^{-1})	R^2
298	56.82	0.06	0.99	18.19	1.23	0.99
308	104.17	0.29	0.98	4.38	2.71	0.82
318	111.11	0.60	0.99	5.07	2.99	0.73

Table S3
Parameters of the pseudo-first-order and the pseudo-second-order for MV adsorption

		Pseudo-first-order model			Pseudo-second-order model		
C_o (mg L^{-1})	$q_{e,exp}$	$k_1 \times 10$ (min^{-1})	$q_{e,cal}$ (mg g^{-1})	R^2	$k_2 \times$ (g mg^{-1} min^{-1})	$q_{e,cal}$ (mg g^{-1})	R^2
25	22.55	0.46	4.26	0.78	1.14	22.88	0.99

Table S4
Thermodynamic parameters of MV adsorption

T (K)	$\Delta G°$ (kJ/mol)	$\Delta H°$ (kJ/mol)	$\Delta S°$ (kJ/mol K)
298	–6.86		
308	–8.52	34.53	0.138
318	–9.62		

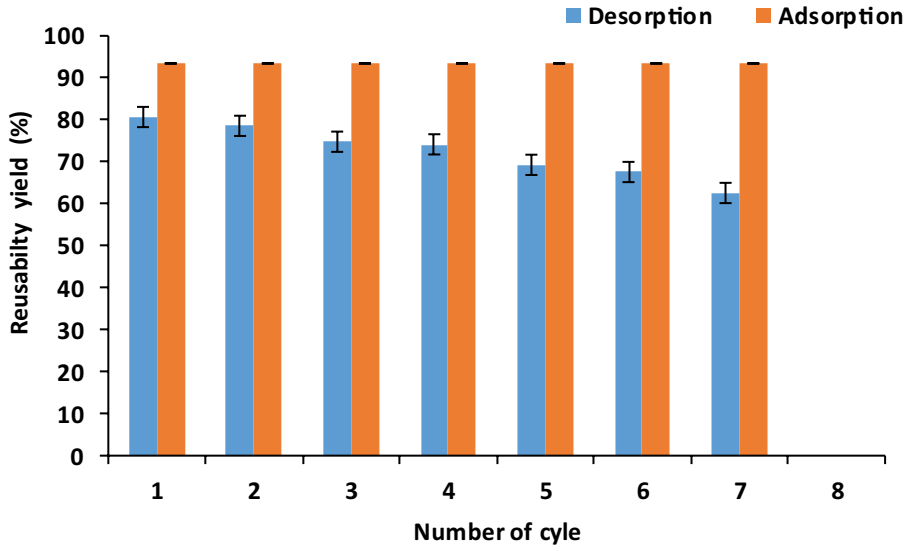

Fig. S3. Recycling performance of the prepared CCZ adsorbent (temperature: 298 K, adsorbent dosage: 0.1 g/100 mL, agitation: 120 rpm, contact time: 60 min, pH: 7).